One neutron transfer reaction spectroscopy of ^{195}Pt as a detailed test of the $U(6/12)$ supersymmetry

A. Metz, Y. Eisermann, A. Gollwitzer, R. Hertenberger, B. D. Valnion, and G. Graw
Ludwig-Maximilians Universität München, Am Coulombwall 1, D-85748 Garching, Germany

J. Jolie
Institut de Physique, University of Fribourg, Pérolles, CH-1700 Fribourg, Switzerland
(Received 30 November 1999; published 18 May 2000)

We investigated the nucleus ^{195}Pt via (p,d) and polarized $(\vec{d},t)$ one neutron pickup reactions. Rather complete spectra are obtained resulting in new spin assignments of 42 states in ^{195}Pt and in information about spectroscopic transfer strengths for each level up to an excitation energy of 1450 keV. A $U(6/12)$ supersymmetric level scheme, describing with its five parameters the $O(6)$ spectrum of ^{194}Pt and the negative parity states of ^{195}Pt, reproduces these spectra. For the lower part of the spectrum also the transfer strengths, calculated with a semimicroscopic transfer operator, agree well with the experiment. The reproduction of the very rich data set improves and extends the evidence that the low-energy spectrum, which results from the coupling of the unpaired neutron in a few, specific orbits to the $O(6)$ core, is determined in a rather complete way by supersymmetry.

PACS number(s): 21.60.Fw, 25.45.Hi

I. INTRODUCTION

In the mid-1970s, Arima and Iachello elaborated for the description of atomic nuclei a remarkably versatile model, the interacting boson model (IBM) [1]. The IBM considers $2N$ valence nucleons which are coupled to N nucleon pairs as $s(l=0)$ and $d(l=2)$ bosons. The even-even nucleus is then described in a space spanned by the irreducible representations (irreps) $[N]$ of $U^B(6)$. The model turned out to be very successful for medium-heavy and heavy nuclei. Moreover, a number of nuclei have low-lying spectra, which resemble in detail one of the three dynamical symmetries of the model. They are denoted by the first subgroup as $SU(3)$, $U(5)$, or $O(6)$ limit. In these cases, the model has an analytic solution.

A further step towards unification was made in the early 1980s when Iachello and co-workers introduced (dynamical) supersymmetry to connect odd-even and even-even nuclei by embedding a Bose-Fermi symmetry into a graded Lie algebra $U(6/M)$ [2,3]. The supersymmetric irrep $[\mathcal{N}]$, then, spanned a space that describes both an even-even nucleus with $\mathcal{N}$ bosons and an odd-A nucleus with $\mathcal{N}-1$ bosons and the odd fermion. If a common set of parameters describes the excited states of two such nuclei, one concludes that the nuclei exhibit a (dynamical) supersymmetry.

An extension of this model was done by Van Isacker *et al.* [4] allowing the description of a quartet of nuclei, using the same algebraic form of the Hamiltonian. This extended supersymmetry (or neutron-proton supersymmetry) deals with boson-fermion and neutron-proton degrees of freedom. The quartet of nuclei consists of an even-even nucleus with $(\mathcal{N}_\nu+\mathcal{N}_\pi)$ bosons, an odd-proton and an odd-neutron nucleus, both with $(\mathcal{N}_\nu+\mathcal{N}_\pi)-1$ bosons, and an odd-odd nucleus with $(\mathcal{N}_\nu+\mathcal{N}_\pi)-2$ bosons. The extended supersymmetry relates the often very complex structure of the odd-odd nucleus to the simpler ones of even-even and odd-A systems.

Recently, strong evidence for the existence of supersymmetry in atomic nuclei has been obtained from the study of the odd-odd nucleus ^{196}Au in ^{197}Au$(\vec{d},t)$, ^{197}Au(p,d), and ^{198}Hg$(\vec{d},\alpha)$ transfer reactions [5]. Within the extended supersymmetry, the low-lying part of the spectrum of odd-odd ^{196}Au follows as a prediction from the reproduction of the spectra of ^{194}Pt within the $O(6)$, of ^{195}Au within the $U(6/4)$ proton, and of ^{195}Pt within the $U(6/12)$ neutron supersymmetry. In all three cases, of course, the even-even core is treated in the same way. In the model, three parameters determine the core, ^{194}Pt, two more are needed to reproduce in addition ^{195}Pt, and a sixth to determine also ^{195}Au. All six parameters then yield a prediction for ^{196}Au.

In view of these very few parameters the reproduction of a rich spectrum as for ^{195}Pt is an important result in itself. Further, the investigation is a main input for the prediction of the spectrum of odd-odd ^{196}Au including the symmetries in a unified $U_\nu(6/12)\times U_\pi(6/4)$ supersymmetry without any further neutron-proton coupling strength parameter. That analysis is an additional, independent, and very fascinating aspect of the importance of group theoretical structures in complex nuclear systems.

In this paper we describe (p,d) and $(\vec{d},t)$ transfer reaction experiments taken in the context of the study presented in [5] with highest energy resolution to improve our experimental knowledge about ^{195}Pt. We also reconsider the actual parametrization of the $U(6/12)$ supersymmetry which relates ^{194}Pt and ^{195}Pt. The reproduction of the data (excitation energies and spectroscopic factors) improves and extends the evidence for the existence of supersymmetry in this atomic nucleus.

The level schemes of ^{194}Pt and ^{195}Pt had been investigated in much detail. Nevertheless, there are safe spin assignments for 21 excited states in ^{195}Pt only, all at excitation energies below 900 keV. Historically, ^{195}Pt was the first experimental candidate of a $U(6/12)$ supersymmetry suggested

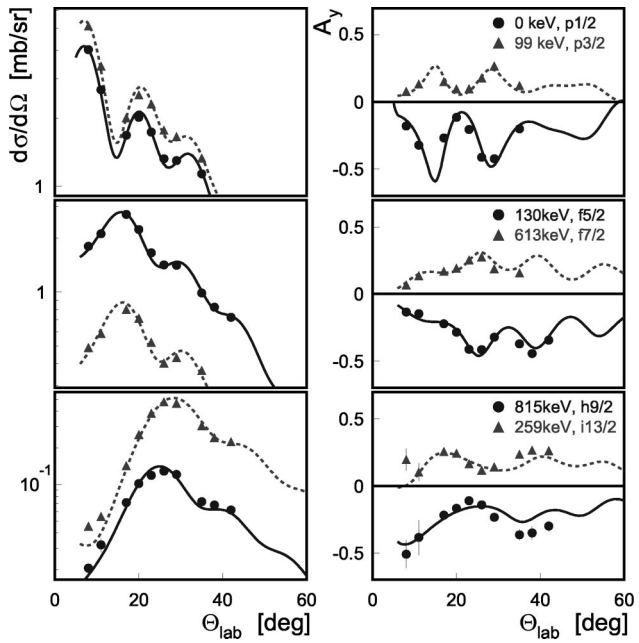

FIG. 1. The ^{196}Pt(p,d) ^{195}Pt spectrum in a logarithmic scale, measured with 26 MeV protons at a scattering angle of 25°, as a function of the excitation energy in the range from 0 to 1500 keV. The resolution is about 4 keV FWHM. States newly resolved are marked by stars.

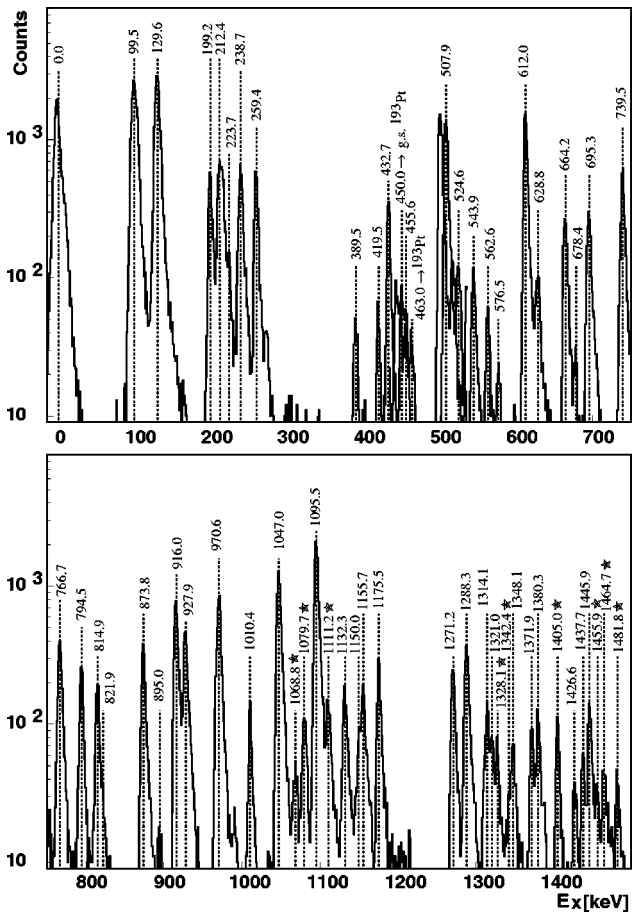

FIG. 2. Measured (points) and calculated (lines) angular distributions of differential cross section (left) and analyzing power (right) of the $(\vec{d},t)$ ^{195}Pt experiment are shown for six different values of transfered l and j.

by Balantekin *et al.* [6]. The $U(6/12)$ multi-j supersymmetry deals with an unpaired neutron which is restricted to the $j=1/2$, 3/2, or 5/2 orbits of identical parity. They interpreted the nucleus in the framework of a $SO^{B+F}(6)\times SU^{F}(2)$ symmetry, assuming the $O(6)$ limit for the boson core. Their work led to a one to one correspondence between the low-lying theoretical and experimental energy levels. This correspondence is quite remarkable, since other theoretical interpretations of the observed spectra, such as the Nilsson model, cannot account for all levels [7].

The supersymmetric relation of even and odd Pt isotopes had been studied in more detail by Sun *et al.* using an improved version of the $U(6/12)$ supersymmetry [8,9]. They described the level scheme of ^{195}Pt, at least qualitatively, up to an energy of 560 keV. Finally, Mauthofer *et al.* [10,11] provided on the basis of their γ spectroscopical information a new interpretation of the ^{195}Pt levels in terms of the $U(6/12)$ quantum numbers, which led to a better agreement of experimental and theoretical energy spectra. In addition, experimental $E2$-decay properties of ^{195}Pt were rather well described in their supersymmetry scheme. Their classification of levels in ^{195}Pt in terms of the $U(6/12)$ quantum numbers up to $\sim$650 keV defined the starting point of our investigation.

II. EXPERIMENTAL STUDY OF ^{195}Pt WITH ONE NEUTRON PICKUP REACTIONS

We studied ^{195}Pt in (p,d) and polarized $(\vec{d},t)$ transfer experiments at the Tandem van-de-Graaff accelerator and the Q3D magnetic spectrograph of the Beschleuniger Laboratorium der Ludwig Maximilians Universität (LMU) and the Technischen Universität (TUM) München [12]. The excellent energetic characteristics of the accelerator, the spectrograph, and the detector imply an intrinsic energy resolution of about $\Delta E\cong 3$ keV FWHM in the detection of outgoing particles. This allows for the measurement of high resolution energy spectra.

The target was a foil of metallic, 97% enriched ^{196}Pt with a thickness of 115 μg/cm^2. The beam intensity was integrated in a Faraday cup, thus absolute cross sections were obtained. The incoming beams, 26 MeV protons and 25 MeV polarized deuterons, respectively, had intensities in the order of a few hundred nA. The outgoing deuterons and tritons from the (p,d) and (d,t) transfer reactions, respectively, were momentum-separated by the Q3D magnetic spectrograph within a solid angle of 10 msr. The focal plane detector consists of an array of single-wire proportional detectors with an additional cathode readout structure, followed by a plastic scintillator for particle identification [13–15]. The device provides control of the detection efficiency which is near one. The polarized deuteron beam was provided by a Lamb-shift negative ion source with spin filter [16], thus the vector polarization of the beam of $\pm 60(3)\%$

TABLE I. Parameters of the optical potentials used in the DWBA calculations in standard notation. In the calcuations a Gaussian finite range correction was applied, using FNRG=0.85.

	V_r [MeV]	V_{so} [MeV]	W_0 [MeV]	W_D [MeV]	r_r [fm]	r_{so} [fm]	r_0 [fm]	r_D [fm]	a_r [fm]	a_{so} [fm]	a_0 [fm]	a_D [fm]	R_c [fm]	nlc
d	104.7	13.1		52.5	1.12	1.0		1.23	0.80	0.66		1.0	1.15	0.54
t	154.7		22.0		1.16		1.44		0.82		0.86		1.25	0.25
n	var.				$\lambda=25$				1.17			0.75		0.85

was interchanged without any effect on the beam position at the target.

Because of the excellent energy resolution (4 keV FWHM, see also Fig. 1), the (p,d) transfer experiment is used to provide the level identification and the energy calibration of the observed states in ^{195}Pt. To obtain information on quantum numbers and excitation strength, we studied the (d,t) reaction. In contrast to (p,d), this reaction is more restricted to the nuclear surface. Thus, the angular distributions of (d,t) show the more pronounced structures. Using a polarized beam, we measured angular distributions of differential cross section and analyzing power. From their very distinct patterns—compare Fig. 2—the determination of the transfered orbital and total angular momenta l and j, with $j=l+1/2$ or $l-1/2$, is obvious. The spectroscopic factors are obtained by comparison to distorted-wave Born approximation (DWBA) calculations. Because of the $J^\pi=0^+$ ground state of the target nucleus ^{196}Pt, the J^π values of the excited states in ^{195}Pt are given directly by the transfered values as $J=j$ and $\pi=(-1)^l$.

For the excitation energy calibration of the (p,d) ^{195}Pt spectrum, we used the excitation energies of 25 levels determined in γ-decay experiments [18] and which were identified also in our spectra. The correlation of channel and excitation energy was achieved for the whole range of 0 to 1500 keV with one polynomial of rank $n=4$. The observed deviations in the energy determination are on the order of 0.5 keV. This is understood as a fluctuation resulting from nonlinearities of the detector cathode readout. The total error of the excitation energies, as determined from our spectra, results from this intrinsic uncertainty and from the error of the Gaussian line fit of the respective state. The calibrated (p,d) ^{195}Pt spectrum is shown in Fig. 1. With respect to the 3% impurity in the ^{196}Pt target, which was about half ^{195}Pt and half ^{194}Pt, we identified the ground state and the first excited state of ^{193}Pt at 450 keV and 464 keV, respectively, in the spectra (compare to Fig. 1).

In the $(\vec{d},t)$ transfer experiment, we measured spectra at ten scattering angles from 8° to 42°. Since the energy resolution of this measurement was not as good as in (p,d), the spectra were analyzed using the information from the (p,d) level scheme to fix the relative positions of the states. As peak shape a Gaussian with an exponential tail on the high energy side was used, thus essentially only the values of the peak integrals were fitted.

For the observed transfers $i_{13/2}$ and $g_{9/2}$ to positive parity states and $p_{1/2}$, $p_{3/2}$, $f_{5/2}$, $f_{7/2}$, and $h_{9/2}$ to negative parity states, DWBA calculations were done using the code CHUCK3. The parameters for the optical potentials of the deuterons and tritons were taken from [19] and [20], respectively. Applying the numerical fit routine MINUIT [21], they are slightly adjusted for optimized agreement with the experiment (compare to Table I). The determination of the respective spectroscopic strengths G_{lj} was done by a fit of the data using the relations

$$\frac{d\sigma}{d\Omega}(\theta)=G_{lj}\sigma^{lj}(\theta)=v_j^2(2j+1)S_{lj}\sigma^{lj}(\theta),$$
$$A_y(\theta)=A_y^{lj}(\theta), \tag{1}$$

with $\sigma^{lj}(\theta)$ and $A_y^{lj}(\theta)$ being the normalized angular distributions from the DWBA calculations, S_{lj} the spectroscopic factor, and v_j^2 the occupation probability of the respective neutron orbit j. In this way we obtain for 62 states up to 1500 keV spin parity and spectroscopic strengths G_{lj}.

Figure 2 shows examples of angular distributions of different lj transfers observed in the experiment and the reproduction in the DWBA calculations (the complete set of data is displayed in [17]). The clear structures of the distributions allows an easy distinction of different lj transfers. In Table II, all information of previous experiments, taken from Nuclear Data Sheets [18], and the results of our transfer experiments are summarized.

The comparison of the data shows that most of the known states in the range of 0 to 1500 keV are resolved in the high resolution (p,d) transfer reaction. Only six positive parity and nine negative parity states are missing, as a result of their low cross sections or of a high level density in the respective energy region. However, more than 15 new states are detected in the energy region above 1 MeV. The main progress obtained from the polarized $(\vec{d},t)$ experiment are the new or now unique spin assignment for 42 levels and the determination of the spectroscopic strengths G_{lj} for 62 levels.

III. SUPERSYMMETRIC CLASSIFICATION OF ^{195}Pt

The $U(6/12)$ supersymmetry scheme was first constructed by Balantekin, Bars, Bijker, and Iachello [6] and extended by Van Isacker, Frank, and Sun [22]. In the latter version, the $U(6/12)$ symmetry was realized in all three limits [$O(6)$, $U(5)$, and $SU(3)$] of the IBM. It treats fermion orbits of a given parity with angular momenta $j=1/2$, 3/2, and 5/2. The respective group chain of the $U(6/12)$ supersymmetry is

TABLE II. Summary of the experimental results for ^{195}Pt from transfer experiments compared with adopted levels of Nuclear Data Sheets (NDS) [18].

NDS		Expt.			Theory		
energy [keV]	J^π	energy [keV]	J^π	G_{lj} [10^{-2}]	energy [keV]	J^π	G_{lj} [10^{-2}]
0.0	$1/2^-$	0.0	$1/2^-$	78.12(22)	0.0	$1/2^-$	59.63
98.882(4)	$3/2^-$	99.5(6)	$3/2^-$	88.72(28)	162.5	$3/2^-$	139.74
129.777(5)	$5/2^-$	129.5(6)	$5/2^-$	209.2(6)	179.6	$5/2^-$	208.39
199.526(12)	$3/2^-$	199.2(6)	$3/2^-$	12.76(12)	244.7	$3/2^-$	4.21
211.398(6)	$3/2^-$	212.4(6)	$3/2^-$	20.60(12)	253.3	$3/2^-$	18.66
222.225(6)	$1/2^-$	223.5(7)	$1/2^-$	14.6(8)	234.4	$1/2^-$	13.61
239.269(6)	$5/2^-$	238.7(6)	$5/2^-$	34.98(24)	270.5	$5/2^-$	80.10
259.30(8)	$13/2^+$	259.4(6)	$13/2^+$	356(25)			
389.16(6)	$5/2^-$	389.5(7)	$5/2^-$	1.44(6)	318.0	$5/2^-$	2.99
419.703(4)	$3/2^-$	419.5(7)	$3/2^-$	0.76(4)	476.5	$3/2^-$	0.49
432.20(8)	$9/2^+$	432.7(6)	$9/2^+$	44.8(4)			
449.66(5)	$(7/2^-)$	450.0(7)	$7/2^-$	1.52(16)	342.9	$7/2^-$	
455.20(4)	$5/2^-$	455.6(7)	$5/2^-$	1.50(12)	493.7	$5/2^-$	1.05
508.08(6)	$5/2^-,7/2^-$	507.9(6)	$7/2^-$	51.12(24)	596.3	$7/2^-$	
524.848(4)	$3/2^-$	524.6(6)	$3/2^-$	0.76(4)	567.4	$3/2^-$	0.27
544.2(6)	$5/2^-$	543.9(6)	$5/2^-$	2.76(6)	584.5	$5/2^-$	0.57
547.27(11)	$11/2^+$	not resolved					
562.81(5)	$9/2^-$	562.6(7)	$9/2^-$	31.4(7)	627.2	$9/2^-$	
590.896(5)	$3/2^-$	not resolved			558.8	$3/2^-$	0.00
612.72(8)	$7/2^-$	612.0(6)	$7/2^-$	51.36(24)	687.1	$7/2^-$	
630.138(8)	$1/2^-,3/2^-$	628.8(7)	$1/2^-$	0.60(4)	548.5	$1/2^-$	0.00
632.1(5)	$1/2^-,3/2^-$	not resolved			581.2	$3/2^-$	0.00
664.200(10)	$5/2^-,7/2^-$	664.2(6)	$5/2^-$	10.92(12)	598.4	$5/2^-$	0.00
667.1(5)	$(9/2^-)$	not resolved			718.0	$9/2^-$	
678(1)	$5/2^-,7/2^-$	678.4(8)	$5/2^-$	0.79(6)	632.0	$5/2^-$	0.00
695.30(6)	$(7/2^-)$	695.3(6)	$7/2^-$	10.64(16)	656.1	$7/2^-$	
739.546(6)	$1/2^-,3/2^-$	739.5(6)	$1/2^-$	11.04(6)	668.9	$1/2^-$	20.01
765.8(9)	$(7/2^-)$	766.7(6)	$7/2^-$	14.80(16)	700.9	$7/2^-$	
793(2)	$11/2^+,13/2^+$	794.5(6)	$13/2^+$	130.9(11)			
793.0(10)	$3/2^-$	not resolved			851.3	$1/2^-$	0.00
814.52(4)	$9/2^-$	814.9(6)	$9/2^-$	119.3(14)	731.9	$9/2^-$	
821.85(6)	$5/2^+$	821.9(12)	$5/2^+$	0.96(6)			
875(1)	$5/2^-,7/2^-$	873.8(6)	$7/2^-$	14.21(16)	970.1	$7/2^-$	
895.42(7)	$9/2^-$	895.0(9)	$9/2^-$	6.10(40)	787.9	$9/2^-$	
915(1)		916.0(6)	$7/2^-$	24.16(16)	1015.0	$7/2^-$	
925(5)	$5/2^-,7/2^-$	$\rightarrow$916.0					
926.89(5)	$1/2^-,3/2^-$	927.9(6)	$3/2^-$	7.92(8)	922.2	$3/2^-$	10.12
930.71	$(9/2^-)$	not resolved			1045.9	$9/2^-$	
971.3	$5/2^-,7/2^-$	970.6(6)	$7/2^-$	29.76(16)	1060.3	$7/2^-$	
1016(5)	$5/2^-,7/2^-$	1010.4(7)	$5/2^-$	5.34(12)	939.4	$5/2^-$	5.72
1049.3(7)		1047.1(7)	$7/2^-$	40.80(24)	1105.8	$7/2^-$	
1058(5)	$5/2^-,7/2^-$						
new		1068.8(7)	$9/2^-$	20.4(8)	1136.7	$9/2^-$	
new		1079.7(7)	$5/2^-$	6.18(12)	1017.1	$5/2^-$	0.00
1091.8(5)	(5/2 to 13/2)	not resolved					
1095.8(4)	$1/2^-,3/2^-$	1095.5(7)	$3/2^-$	34.44(12)	977.5	$3/2^-$	0.00
new		1111.2(7)	$7/2^-$	2.72(16)	1074.8	$7/2^-$	
1122.66(6)	$3/2^+,5/2^+$	not resolved					
1132.40(2)	$1/2^-,3/2^-$	1132.3(7)	$1/2^-$	3.30(4)	967.2	$1/2^-$	0.00

TABLE II. (*Continued*)

NDS		Expt.			Theory		
energy [keV]	J^π	energy [keV]	J^π	G_{lj} [10^{-2}]	energy [keV]	J^π	G_{lj} [10^{-2}]
1151(6)	$1/2^-,3/2^-$						
new		1150.0(8)	$9/2^+$	1.2(6)			
1155.8		1155.7(8)	$5/2^-$	8.58(24)	1050.7	$5/2^-$	0.00
1160.38	$1/2^-,3/2^-$	not resolved			999.9	$3/2^-$	0.00
1166.4	$1/2^+,3/2^+$	not resolved					
1189(6)	$5/2^-,7/2^-$	1175.5(8)	$7/2^-$	9.28(16)	1119.7	$7/2^-$	
1271.0(3)	$1/2^-,3/2^-$	1271.2(9)	$3/2^-$	3.40(4)	1236.3	$3/2^-$	0.06
1287.7(4)	$1/2^-,3/2^-$	1288.3(9)	$1/2^-$	2.56(8)	1350.7	$1/2^-$	5.24
new		1288.3(9)	$5/2^-$	8.22(30)	1253.5	$5/2^-$	0.13
1294(1)	$1/2^-,3/2^-$	$\rightarrow$1288.3					
1306(10)							
1312.7(7)	$1/2^+,3/2^+$	not resolved					
new		1314.1(10)	$5/2^-$	5.76(12)	1361.5	$5/2^-$	0.04
1320.8(4)	$1/2^-,3/2^-$	1321.0(10)	$3/2^-$	0.64(4)	1344.3	$3/2^-$	0.05
new		1328.1(10)	$13/2^+$	33.7(10)			
1334.7(4)	$1/2^-,3/2^-$	not resolved			1418.6	$3/2^-$	0.00
new		1342.4(13)	$5/2^-,7/2^-$	0.96(8)	1435.8	$5/2^-$	0.00
1346.9(6)	1/2,3/2	not resolved					
new		1348.2(11)	$5/2^+$	1.14(6)			
1372.7(4)	$1/2^-,3/2^-$	1371.9(12)	$3/2^-$	1.48(4)	1426.6	$3/2^-$	0.51
1378(10)	$11/2^+,13/2^+$	1380.3(12)	$13/2^+$	57.1(11)			
new		1405.0(13)	$13/2^+$	50.7(10)			
1411.1(5)	$1/2^-,3/2^-$	not resolved					
1425.0(5)	$1/2^-,3/2^-$	not resolved					
new		1426.6(14)	$7/2^-$	1.52(8)	1356.1	$7/2^-$	
1438.3(4)	1/2,3/2	1437.7(14)	$1/2^-$	1.28(4)	1416.3	$1/2^-$	1.63
1445.3(5)	$1/2^-,3/2^-$	1445.9(14)	$3/2^-$	1.72(4)			
new		1455.9(14)	$7/2^-$	0.56(8)			
new		1464.7(15)	$5/2^-$	1.86(12)	1499.8	$5/2^-$	0.36
new		1473.2(15)	$3/2^-$	0.48(4)			
new		1510.7(15)					
new		1516.3(15)	$7/2^-$	3.36(8)			
new		1524.7(15)	$13/2^+$	19.0(10)			
new		1539.3(15)	$7/2^-$	3.76(8)			
new		1552.7(15)					
new		1559.7(17)					
new		1579.4(16)					
new		1592.5(17)					

$$
\begin{array}{ccccccc}
U(6/12) & \supset & U^B(6) & \times & U^F(12) & \supset & \\
\downarrow & & \downarrow & & \downarrow & & \\
|\mathcal{N}\} & & [N] & & [1^m] & &
\end{array}
$$

$$
\begin{array}{ccccccc}
U^B(6) & \times & U^F(6) & \times & U^F(2) & \supset & \\
\downarrow & & \downarrow & & \downarrow & & \\
[N] & & [1^m] & & [1^m] & &
\end{array}
$$

$$
\begin{array}{ccccccc}
U^{B+F}(6) & \times & SU^F(2) & \supset & O^{B+F}(6) & \times & SU^F(2) \supset \\
\downarrow & & \downarrow & & \downarrow & & \downarrow \\
[N_1,N_2] & & s & & \langle \sigma_1,\sigma_2 \rangle & & s
\end{array}
$$

$$
\begin{array}{ccccccc}
O^{B+F}(5) & \times & SU^F(2) & \supset & O^{B+F}(3) & \times & SU^F(2) \supset \\
\downarrow & & \downarrow & & \downarrow & & \downarrow \\
(\tau_1,\tau_2) & & s & & L & & s
\end{array}
$$

$$
\begin{array}{c}
\mathrm{Spin}(3) \\
\downarrow \\
J.
\end{array}
$$

If one constructs the Hamiltonian, neglecting those Casimir operators contributing only to the binding energy of a nucleus, five second-order Casimir operators with their five parameters remain and the Hamiltonian reads

$$
\begin{aligned}
H = & AC_2(U^{B+F}(6)) + BC_2(O^{B+F}(6)) \\
& + CC_2(O^{B+F}(5)) + DC_2(O^{B+F}(3)) + EC_2(spin(3)).
\end{aligned} \tag{2}
$$

The energy E of the eigenstates is then an analytic expression as a function of the relevant quantum numbers and reads

$$
\begin{aligned}
E = & A[N_1(N_1+5) + N_2(N_2+3)] + B[\sigma_1(\sigma_1+4) \\
& + \sigma_2(\sigma_2+2)] + C[\tau_1(\tau_1+3) + \tau_2(\tau_2+1)] \\
& + DL(L+1) + EJ(J+1).
\end{aligned} \tag{3}
$$

The Hamiltonian describes both an even-even and an odd-even nucleus with the same parameters. The quantum numbers in the Hamiltonian are directly derived from the reduction rules within the group chain and are displayed in Fig. 4 where the theoretical and experimental level schemes of ^{194}Pt and ^{195}Pt are compared. We separate the supersymmetric level scheme into six different bands according to their quantum numbers. They are referred to as follows:

$$B^{\langle 7,0\rangle}_{[7,0]}:[7,0]\langle 7,0\rangle,$$

$$B^{\langle 6,1\rangle}_{[6,1]}:[6,1]\langle 6,1\rangle(\tau_1,0),$$

$${}^2B^{\langle 6,1\rangle}_{[6,1]}:[6,1]\langle 6,1\rangle(\tau_1,1),$$

$$B^{\langle 5,0\rangle}_{[6,1]}:[6,1]\langle 5,0\rangle,$$

$$B^{\langle 4,1\rangle}_{[6,1]}:[6,1]\langle 4,1\rangle,$$

and

$$B^{\langle 5,0\rangle}_{[7,0]}:[7,0]\langle 5,0\rangle,$$

respectively (compare Fig. 4).

Mauthofer *et al.* classified the levels at 667 keV, 612 keV, 563 keV, 508 keV, 239 keV, 212 keV, 130 keV, and 99 keV with respect to their $B(E2)$ branching ratios. This automatically fixed most quantum numbers of the neighboring states with respect to their energies and angular momenta. Additionally, they proposed that the levels at 927 keV, 1132 keV, and 1156 keV are the three lowest states of the $B^{\langle 5,0\rangle}_{[6,1]}$ band. Comparing the new spin assigments from the polarized $(\vec{d},t)$ transfer experiment, it turns out that this last classification was wrong. The obtained spin sequence of $3/2^-$ and $1/2^-$ for the states 927 keV and 1132 keV is exactly opposite as proposed. Inspecting the new level scheme, only one possible set of $1/2^-$, $3/2^-$, and $5/2^-$ states is detected at the energies of 740 keV, 927 keV, and 1010 keV, which fits to the $B^{\langle 5,0\rangle}_{[6,1]}$ band. This result, also supported by the comparison of the experimental and theoretical spectroscopic strengths discussed below, changes significantly the value of the the parameter A of the $U(6/12)$ Hamiltonian.

IV. CALCULATION OF THE TRANSFER STRENGTHS

In order to provide a theoretical prediction of transfer strengths, one needs to define the theoretical transfer operator. In all supersymmetric calculations made up to now, the transfer operator between nuclei having the same number of bosons N for simplicity was taken to be the operator $a^\dagger_j$ which in the supersymmetric model creates a fermion. The advantage of this simple operator is that analytic results can be easily derived [23]. However, due to selection rules implied by this kind of operator, the transfer operator provides a poor description of the observed fragmentation of the strength [24].

To apply a more realistic operator, we use as in the IBFA [25] a semimicroscopic transfer operator obtained from the mapping of the single-nucleon creation operator onto the boson-fermion space to account for the experimental situation, the transfer of a nucleon. This yields in the case of a hole

$$
\begin{aligned}
\mathcal{T}^{lj} = & \frac{v_j a^\dagger_j}{K_\alpha} - \sum_{j'} \sqrt{\frac{10N_\pi}{(2j+1)N^2}} u_j(u_j v_{j'} + v_j u_{j'}) \\
& \times \left\langle \frac{1}{2} l' j' \middle| Y_2 \middle| \frac{1}{2} lj \right\rangle s^\dagger(\tilde{d} a^\dagger_{j'})^{(j)} \frac{1}{K_\alpha} \frac{1}{K_\beta},
\end{aligned} \tag{4}
$$

with $u_j^2 = 1 - v_j^2$. K_α and K_β are normalization constants, being functions of the u_j^2, as described in [25]. The implementation of this operator in the numerical code is discussed in the Appendix. The semimicroscopic operator contains the simple operator as a first approximation. Both depend on the same number of parameters v_j. These parameters are not free but can be obtained from the experiment. In our case, we obtained $v^2_{1/2} = 0.49(10)$, $v^2_{3/2} = 0.43(10)$, and $v^2_{5/2}$

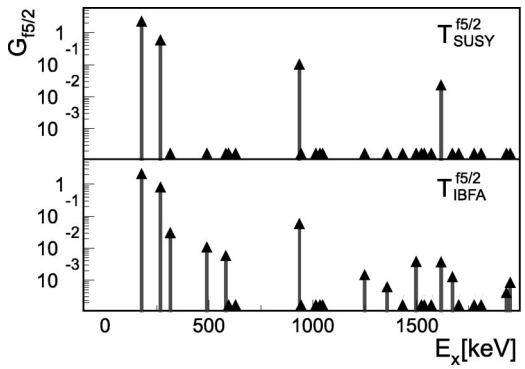

FIG. 3. Comparison of the theoretically calculated $G_{f5/2}$ transfer strengths using the simple fermion creation operator (upper part) and the semimicroscopic nucleon creation operator (lower part). The arrows show the predicted strength on a logarithmic scale.

$=0.51(10)$ from the summed transfer strengths observed in the ^{196}Pt$(\vec{d},t)$ ^{195}Pt reaction in the range 0 to 1500 keV. The second term in Eq. (3) induces the additional fragmentation. The derivation of the operator $\mathcal{T}^{lj}$ is accomplished by mapping the IBFA single-nucleon creation and annihilation operators and by excluding all irrelevant terms [26]. In this series, terms of the type $(sd^{\dagger}a^{\dagger}_{j'})^{(j)}$ do not appear because they correspond to a change of the seniority ν in the fermion space by three units while for a single particle operator one has $|\Delta\nu|=1$.

The correlation between the microscopic fermion space and the boson space is provided by the fermion seniority ν which can be directly connected to the $O(5)$ quantum number τ [26]. Since the $O(5)$ quantum number is a good quantum number in the $U(5)$ and the $O(6)$ limit of the IBM [27], the transfer operator $\mathcal{T}^{lj}$ follows some selection rules for $O(5)$. At the level of the $O(6)$ symmetry such selection rules do not appear because the operator has no definite tensorial $O(6)$ character.

Therefore, the selection rules of the σ-quantum numbers of the $O(6)$ are broken by the transfer operator while the selection rules for the τ-quantum number of the $O(5)$ group are still valid. The combination of the $sd^{\dagger}$ with the $a^{\dagger}_j$ operator in the semimicroscopic transfer operator thus leads only to selection rules for (τ_1,τ_2). In essence, each term in the transfer operator can be rewritten in terms of a linear combination of operators having the $O(5)$ tensorial characters (2,0), (1,0), (0,0), or (1,1). As a result of this property and considering the tensorial character $\tau=0$ of the initial state, only states with

$$\begin{aligned}&(\tau_1=0;\tau_2=0),\\ &(\tau_1=1;\tau_2=0),\\ &(\tau_1=2;\tau_2=0),\\ &(\tau_1=1;\tau_2=1)\end{aligned}\qquad(5)$$

can be populated in the odd-even nucleus.

Figure 3 compares the results obtained for the $G_{f5/2}$ transfer strengths using the simple fermion creation operator and the semimicroscopic operator. One clearly notices that with the latter the strength is distributed over many more states. Due to the above mentioned selection rules this is especially true for the lower part of the spectrum.

TABLE III. Parameter set of the supermultiplet ^{194}Pt and ^{195}Pt according to Eq. (3). The parameters are obtained by a least-squares fit of 53 ^{195}Pt and the eight ^{194}Pt experimental levels.

A	*B*	*C*	*D*	*E*
48.7 keV	−42.2 keV	52.3 keV	5.6 keV	3.4 keV

V. COMPARISON WITH EXPERIMENT

In order to obtain a complete level by level classification, we first compared the measured and predicted spectroscopic strengths of the $1/2^-$, $3/2^-$, and $5/2^-$ states and related them to the $U(6/12)$ classification, accordingly. The remaining negative parity states $(7/2^-,9/2^-)$ were classified afterwards with respect to their energies and angular momenta. The parameters $A,\ldots,E$ of the Hamiltonian were obtained by a least-squares fit including 53 levels of ^{195}Pt and eight levels of ^{194}Pt. The final parameter set is displayed in Table III and the quantum number classification of the energy levels of ^{195}Pt is shown in Fig. 4. Since the spectroscopic transfer strengths G_{lj} from the semimicroscopic transfer operator yield for many states a definite correlation of predicted and measured states, a one-to-one correlation between theory and experiment was observed. Table II gives a detailed comparison of theoretical and experimental transfer strengths.

For more detail, the obtained correlation of the eight experimentally known $1/2^-$ states and the calculated states of the $U(6/12)$ supersymmetry is displayed in Fig. 5 in a logarithmic plot of the respective experimental (upper part) and theoretical (lower part) transfer strengths as a function of excitation energy. The one-to-one level correlation of the prediction with the experiment is shown by arrows. The states connected by a dashed arrow are the ones with theoretically predicted zero transfer strength because of the selection rules of the transfer operator.

For the states at 0 keV, 224 keV, 740 keV, 1288 keV, and 1438 keV, the classification is definite due to the agreement of observed and calculated transfer strengths. The two states at 629 keV and 1132 keV are correlated to states with $(\tau_1=2,\tau_2=1)$ in the ${}^2B^{\langle 6,1\rangle}_{[6,1]}$ band, thus they are not described by the semimicroscopic transfer operator according to Eq. (5). The 793 keV state was not resolved in the (p,d) and $(\vec{d},t)$ transfer experiments. It is known from Coulomb excitation experiments [28] and was assigned as a $3/2^-$ state [18], using the multi-j supersymmetry scheme of Mauthofer *et al.* We reassigned this state as $1/2^-$ with respect to our new and complete supersymmetric scheme.

In Fig.6, the theoretical and experimental $G_{p3/2}$ values are compared. Except for the 1096 keV level, all states observed in the transfer experiments are consistently correlated to the supersymmetric scheme with respect to their detected trans-

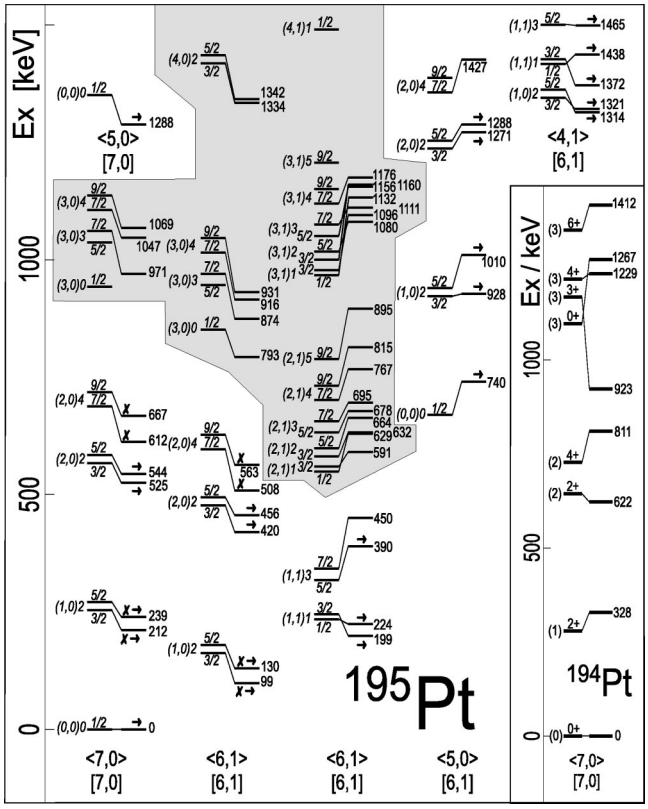

FIG. 4. The classification of the ^{195}Pt (negative parity) and ^{194}Pt states with respect to their $U(6/12)$ quantum numbers. Bands are distinguished by their $\langle \sigma_1, \sigma_2 \rangle$ and $[N_1, N_2]$ quantum numbers. In each band the quantum numbers (τ_1, τ_2) L are indicated on the left side and the spin on top of the predicted energy levels. The corresponding experimental levels with their excitation energies in keV are shown on the right side of the respective predicted level. Levels where the classification is supported by the transfer strengths or by $B(E2)$ ratios are marked by arrows and crosses, respectively. The results for ^{194}Pt are plotted in the additional box to the right. All 53 experimentally known negative parity states of ^{195}Pt up to an energy of 1440 keV are included in this supersymmetric level scheme. The states in the gray shaded area are not described by the semimicroscopic transfer operator due to its selection rules.

fer strength. The 1096 keV state is correlated to the $B^{\langle 6,1 \rangle}_{[6,1]}$ band according to its spin and excitation energy. Furthermore, from the Nuclear Data Sheets [18], four additional states are known (591 keV, 632 keV, 1160 keV, 1335 keV) which are not observed in our experiment. The first one was assigned as $3/2^-$, the other ones as $1/2^-$ or $3/2^-$. With respect to the matching with the calculated level scheme, we relate these four states to the $3/2^-$ states in the bands $B^{\langle 6,1 \rangle}_{[6,1]}$ and $^2B^{\langle 6,1 \rangle}_{[6,1]}$ with τ-quantum numbers not described by the transfer operator. This implies a spin assignment for the three states mentioned due to their consistent inclusion in the level scheme (compare Table II). One should notice that the state at 1096 keV has a remarkable experimental transfer strength which is not described in the model. This might be an indication that an extension of the transfer operator could still improve the achieved agreement of theory and experiment.

In Fig. 7 the experimentally observed $5/2^-$ states and

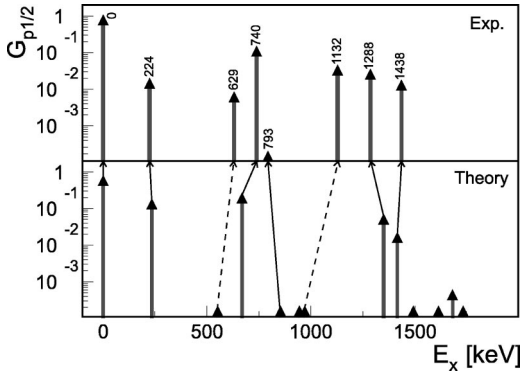

FIG. 5. Comparison of the experimental (upper plot) and theoretically calculated (lower plot) $G_{p1/2}$ transfer strengths. The arrows show the one-to-one level correlation of prediction and experiment. The states, connected by a dashed arrow to the respective experimental level, have no predicted transfer strength because of the selection rules of the transfer operator.

their respective transfer strengths are presented. The assignments of these states are safe except for the 1342 keV state, where the data are not sufficient to determine the j-quantum number (while $l=3$). We obtain a consistent correlation of predicted and observed transfer strengths. Vanishing transfer strengths are predicted for the states related to the $^2B^{\langle 6,1 \rangle}_{[6,1]}$ and $B^{\langle 6,1 \rangle}_{[6,1]}$ band. They are related to the experimental states at 664 keV, 678 keV, 1080 keV, 1156 keV, and 1342 keV implying again a tentative spin assignment for the latter state (compare Table II: $5/2^-$,$7/2^-$). The integrated strengths $\Sigma G_{lj}/(2j+1)$ over the 0 keV to 1500 keV range of excitation energy (compare Table II) of the $1/2^-$, $3/2^-$, $5/2^-$, and $7/2^-$ transfers are 0.56, 0.43, 0.50, and 0.32, respectively (with an estimated systematic uncertainty of 20%). As their strength weighted average in excitation energies we obtain 185 keV, 414 keV, 242 keV, and 822 keV in the interval, respectively. The high value for the $p_{3/2}$ transfer is partly correlated to the abnormal 1096 keV state with high transfer strength.

The energy difference between the centers of gravity of the $p_{1/2}$ and $p_{3/2}$ states obtained from data is much smaller than spin-orbit splitting as observed in single particle spectra of ^{207}Pb, for instance, where $p_{1/2}$ and $p_{3/2}$ are split by 900 KeV. The observed smaller value is related to the mass de-

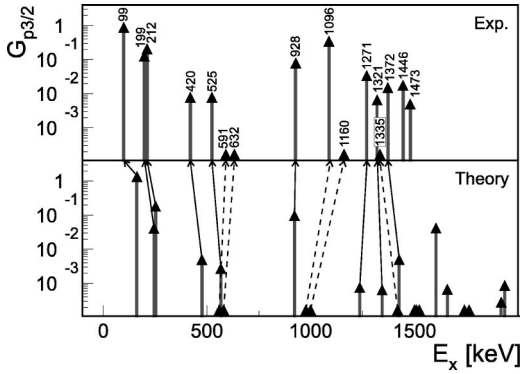

FIG. 6. The $G_{p3/2}$ transfer strengths; compare also the caption of Fig. 5.

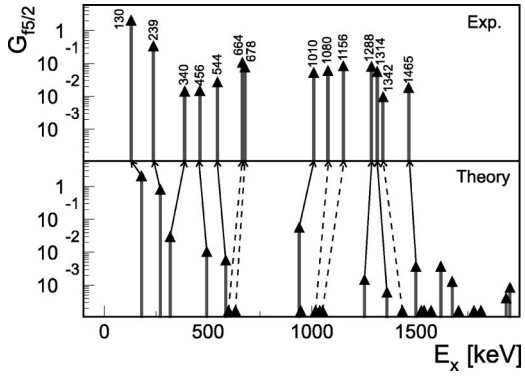

FIG. 7. The $G_{f5/2}$ transfer strengths; compare also the caption of Fig. 5.

pendence of the potential experienced by the nucleons and the different filling of the neutron orbits that affects the relative position. This is discussed in detail by Kisslinger and Sorensen [29]; compare their Fig. 8.

The observed $7/2^-$ strength is about 40% weaker than the $1/2^-$, $3/2^-$, and $5/2^-$ strengths, and the centroid of the $7/2^-$ strength is separated by about 500 keV or more from the scarcely spaced centroids of the $1/2^-$, $3/2^-$, and $5/2^-$ strengths.

The supersymmetric model considers the $1/2^-$, $3/2^-$, and $5/2^-$ orbitals, only. The observed weaker strength and higher excitation energy of the $7/2^-$ orbital is in the line of this approximation. However, one has to expect some mixing of the supersymmetric states with those configurations which include the $7/2^-$ orbital. The mixing causes the nonvanishing spectroscopic factors we observed for the $7/2^-$ states. In addition, it will cause some shifts in the excitation energies, especially at higher excitation energies, and it will generate additional states. The undisturbed states are expected near the energy of the undisturbed $7/2^-$ orbital, that is, above 800 keV plus the energy of the core excitation which is 328 keV for the 2_1^+ and 811 keV for the 4_1^+ excitation. Thus, e.g., for the $1/2^-$ states which derive from the $7/2^-$ orbital only by coupling with the 4^+ core excitation, no additional states are expected in our energy range, and one may expect full verification of the model at low energies, especially for the $1/2^-$ band head states.

The achieved supersymmetric cassification in Fig. 4 shows all predicted energy levels of the $1/2^-$ to $9/2^-$ states of the $U(6/12)$ supersymmetry up to an energy of 1500 keV and the corresponding experimental levels, as discussed. These levels from the Nuclear Data Sheets [18] and in addition the levels resolved in the transfer experiments are in fact all known excited states up to an energy above 1450 keV. In the figure the N- and σ-quantum numbers are written below each band while the $(\tau_1,\tau_2)L$-quantum numbers are indicated to the left of the respective theoretical energy levels with their angular momentum value j given on top. The levels experimentally obtained are marked by their excitation energy on the right and correlated to the respective theoretical states by thin lines. States identified with respect to their transfer strengths are marked by a ''polarization'' arrow on top of the energy level, and to branching ratios marked by a cross. In the individual bands one observes a regular behavior of the states. For instance, in the $B^{\langle 7,0\rangle}_{[7,0]}$ and $B^{\langle 6,1\rangle}_{[6,1]}$ band, all theoretical levels are too high with respect to the measurement while in the ${}^2B^{\langle 6,1\rangle}_{[6,1]}$ band the calculated energies are too low. It is obvious that the predicted level sequences follow almost exactly the measured ones over the whole energy range. Only in the ${}^2B^{\langle 6,1\rangle}_{[6,1]}$ band, the sequence of the levels with $\tau_1=3$ is disturbed. For example, the 629 keV state with spin $1/2^-$ is too high in energy. For nearly all predicted levels of the $U(6/12)$ supersymmetry scheme, a respective experimental state is determined. Only the partners of the $(3,0)0\ \frac{1}{2}^-$ and $(3,0)3\ \frac{5}{2}^-$ states in the $B^{\langle 7,0\rangle}_{[7,0]}$ band and the $(3,0)3\ \frac{5}{2}^-$ state in the $B^{\langle 6,1\rangle}_{[6,1]}$ are still missing. Yet due to the regularity in the scheme, one can predict their excitation energies. For instance, the $1/2^-$ state should be in the range of 800 to 900 keV.

VI. SUMMARY AND CONCLUSIONS

Based on the data of the literature and the high resolution (p,d) and the polarized $(\vec{d},t)$ ^{195}Pt transfer data, we achieved a complete and definite classification of all known negative parity energy levels of ^{195}Pt up to $E_x=1440$ keV. These are 53 states, to a $U(6/12)$ supersymmetric scheme. This satisfying result was achieved in part due to the use of the microscopically derived transfer operator for the calculation of the theoretical spectroscopic transfer strengths. The improved transfer operator, the new parametrization of the $U(6/12)$ Hamiltonian, and the complete classification of ^{195}Pt provided the basis for the description of the odd-odd nucleus ^{196}Au in the framework of the IBM extended supersymmetry of Refs. [5,30].

However, the complete supersymmetric classification of ^{195}Pt and the detailed reproduction of transfer strengths is an important result in itself. It establishes considerably the evidence that supersymmetry exists in the low-energy spectra of even-odd nuclei.

ACKNOWLEDGMENTS

This work was supported by the Swiss National Science Fund and the Deutsche Forschungsgemeinschaft (Grant No. IIC4 Gr 894/2). A.M. acknowledges the financial support of the University of Fribourg during an extended stay. Many enlightening discussions with J. Gröger, C. Günther, and F. Iachello are acknowledged.

APPENDIX: TEST OF THE NUMERICAL CALCULATION

The wave function of the even-even target nucleus ^{196}Pt can be labeled with the IBM-1 quantum numbers of the $O(6)$ limit: $|N\langle\Sigma\rangle n_\Delta(\tau=0)L=0\rangle$, the odd-even nucleus ^{195}Pt is then described by a combination of even-even core states to which an additional fermion $a^\dagger_{j_\nu}$ is coupled to the final spin J: $[|N\langle\Sigma\rangle n_\Delta(\tau)L\rangle\times a^\dagger_{j_\nu}]^{(J)}$. For the numerical calculation the $U(5)$ basis is used. Thus the $O(6)$ wave functions are expanded in the $U(5)$ wave functions: $|Nn_d(v)\alpha L\rangle$. In this framework, the reduced transfer-matrix

element for the operator $[(s^\dagger\tilde{d})^{(2)}a^\dagger_{j'}]^{(j)}$ results as

$$[\langle Nn_d(v)\alpha L|\times a^\dagger_{j_\nu}]^{(J)}\|[(s^\dagger\tilde{d})^{(2)}a^\dagger_{j'}]^{(j)}\|Nn'_d(0)00\rangle$$
$$= -\delta_{j,J}\delta_{j_\nu,j'}\delta_{n'_d,n_d+1}\delta_{L,2}\sqrt{\frac{2j+1}{5}}$$
$$\times\langle Nn_d(v)\alpha 2\|(s^\dagger\tilde{d})^{(2)}\|Nn'_d(0)00\rangle. \quad \text{(A1)}$$

The result (A1) was implemented in the computer program which calculates the $(s^\dagger\tilde{d})^{(2)}$ matrix element numerically [31].

Since the introduction of the new operator in the numerical code is a delicate operation, it is extremely important to have an independent analytical result to test the code. Therefore, we derive an analytical solution in the following. A test of the numerical calculations is provided by the analytical example for the transfer to the second $1/2^-_2$ state of the odd-even nucleus $[|[N,1]\langle N,1\rangle(1,1)1\frac{1}{2}\rangle$ in $U(6/12)$ quantum numbers]. In Ref. [22], Table XV, the wave function of the $1/2^-_2$ state is given as

$$\sqrt{\frac{3}{5}}[|[N]\langle N\rangle(1)2\rangle\times a^\dagger_{3/2}]^{(1/2)}$$
$$+\sqrt{\frac{2}{5}}[|[N]\langle N\rangle(1)2\rangle\times a^\dagger_{5/2}]^{(1/2)}. \quad \text{(A2)}$$

This state is thus exclusively populated by the operator $[(s^\dagger\tilde{d})^{(2)}a^\dagger_{j'}]^{(j)}$. One derives for the transfer matrix element $\mathcal{T}_{fi}(0^+_1\rightarrow 1/2^-_2)$

$$\mathcal{T}_{fi}(0^+_1\rightarrow 1/2^-_2)=\frac{2}{5}\frac{\sqrt{30N_\pi}}{NK_\beta}u_{1/2}\left[\frac{\beta_{3/2,1/2}}{2}+\frac{\beta_{5/2,1/2}}{\sqrt{6}}\right]$$
$$\times\langle 2^+_1\|(s^\dagger\tilde{d})^{(2)}\|0^+_1\rangle. \quad \text{(A3)}$$

The last matrix element to be calculated is described by Van Isacker *et al.* in Ref. [32] and equals

$$\langle 2^+_1\|(s^\dagger\tilde{d})^{(2)}\|0^+_1\rangle=\frac{\sqrt{N(N+4)}}{2(N+1)}\sqrt{\frac{1}{2}}(N-1)\sqrt{5}. \quad \text{(A4)}$$

This analytical result for the transfer matrix element is consistent with the numerically calculated values, which validates the extended computer code IBFFMTR [31].

[1] F. Iachello and A. Arima, *The Interacting Boson Model* (Cambridge University, Cambridge, 1987).
[2] F. Iachello, Phys. Rev. Lett. **44**, 772 (1980).
[3] A.B. Balantekin, I. Bars, and F. Iachello, Nucl. Phys. **A370**, 284 (1981).
[4] P. Van Isacker, J. Jolie, K.L.G. Heyde, and A. Frank, Phys. Rev. Lett. **54**, 653 (1985).
[5] A. Metz, J. Jolie, G. Graw, R. Hertenberger, J. Gröger, C. Günther, N. Warr, and Y. Eisermann, Phys. Rev. Lett. **83**, 1542 (1999).
[6] A.B. Balantekin, I. Bars, R. Bijker, and F. Iachello, Phys. Rev. C **27**, 1761 (1983).
[7] D.D. Warner, R.F. Casten, M.L. Stelts, H.G. Börner, and G. Barreau, Phys. Rev. C **28**, 2521 (1983).
[8] H.Z. Sun, A. Frank, and P. Van Isacker, Phys. Rev. C **27**, 2430 (1983).
[9] H.Z. Sun, M. Valliéres, D.H. Feng, R. Gilmore, and R.F. Casten, Phys. Rev. C **29**, 352 (1984).
[10] A. Mauthofer, K. Stelzer, Th.W. Elze, Th. Happ, J. Gerl, A. Frank, and P. Van Isacker, Phys. Rev. C **39**, 1111 (1989).
[11] A. Mauthofer, K. Stelzer, J. Gerl, Th.W. Elze, Th. Happ, G. Eckert, T. Faestermann, A. Frank, and P. Van Isacker, Phys. Rev. C **34**, 1958 (1986).
[12] W. Assmann, J. de Boer, U. Meyer-Berkout, S. Skorka, E. Huenges, P. Kienle, H. Morinaga, E. Nolte, H. Münzer, L. Rohrer, and H. Schnitter, Nucl. Instrum. Methods **122**, 191 (1974).
[13] R. Hertenberger, H. Kader, F. Merz, J. Eckle, and G. Graw, Nucl. Instrum. Methods Phys. Res. A **258**, 201 (1987).
[14] H. Wessner, R. Hertenberger, H. Kader, and G. Graw, Nucl. Instrum. Methods Phys. Res. A **286**, 175 (1990).
[15] E. Zanotti, M. Bisenberger, R. Hertenberger, H. Kader, and G. Graw, Nucl. Instrum. Methods Phys. Res. A **310**, 706 (1991).
[16] P. Schiemenz, F.J. Eckle, G. Eckle, G. Graw, H. Kader, and F. Merz, in *Proceedings of the Sixth International Symposium on Polarization Phenomena in Nuclear Physics*, edited by M. Kondo, S. Kobayashi, M. Tanifuji, T. Yamazaki, K.-I. Kubo, and N. Onishi (Physical Society of Japan, Tokyo, 1985), p. 1056.
[17] A. Metz, Ph.D. thesis, Ludwig Maximilians Universität, München (1999).
[18] Zhou Chumnei, Nucl. Data Sheets **71**, 367 (1994).
[19] W.W. Daehnick, J.D. Childs, and Z. Vrcelj, Phys. Rev. C **21**, 2253 (1980).
[20] R.P. Ward and P.R. Hayes, At. Data Nucl. Data Tables **49**, 315 (1991).
[21] F. James *et al.*, CERN Program Library D506 (1994).
[22] P. Van Isacker, A. Frank, and H.Z. Sun, Ann. Phys. (N.Y.) **157**, 183 (1984).
[23] J. Jolie, U. Mayerhofer, T. von Egidy, H. Hiller, J. Klora, H. Lindner, and H. Trieb, Phys. Rev. C **43**, R16 (1991).
[24] G. Rotbard, G. Berrier, M. Vergnes, S. Fortier, J. Kalifa, J.M. Maison, L. Rosier, J. Vernotte, P. Van Isacker, and J. Jolie, Phys. Rev. C **47**, 1921 (1993).
[25] O. Scholten and T. Ozzello, Nucl. Phys. **A424**, 221 (1984).
[26] O. Scholten, thesis, University of Groningen (1980).
[27] J. Jolie and H. Lehmann, Phys. Lett. B **342**, 1 (1995).

[28] R.G. Kulkarni and K. Andhradev, Acta Phys. Acad. Sci. Hung. **52**, 199 (1982).
[29] L.S. Kisslinger and R.A. Sorensen, Rev. Mod. Phys. **35**, 853 (1963).
[30] A. Metz, J. Jolie, G. Graw, R. Hertenberger, J. Gröger, C. Günther, N. Warr, and Y. Eisermann (unpublished).
[31] J. Jolie and P. Van Isacker, computer code IBFFMTR (unpublished).
[32] P. Van Isacker, A. Frank, and J. Dukelsky, Phys. Rev. C **31**, 671 (1985).